Desalination and Water Treatment
www.deswater.com

doi: 10.5004/dwt.2022.28258

253 (2022) 100–112
March

Modified attapulgite for phosphorus removal from glyphosate by-product salt solution

Qisheng Wu[a,*], Ming Jiang[a], Weijian Zhang[a], Tao Jiang[a], Mifen Cui[b], Benjun Xi[c], Qingwen Han[c]

[a]*College of Materials Science and Engineering, Yancheng Institute of Technology, Yancheng, 224051, PR China, emails: qishengwu@ycit.cn (Q. Wu), 1779965378@qq.com (M. Jiang), 835584559@qq.com (W. Zhang), 644889552@qq.com (T. Jiang)*
[b]*Colleage of Chemical Engineering Institute, Nanjing University of Technology, Nanjing 210005, China, email: 19792282@qq.com*
[c]*Hubei Xingfa Chemical Group Co., Ltd., Yichang 443711, China, emails: hubeixfjt@126.com (B. Xi), hanqingwen1989@xingfagroup.com (Q. Han)*

Received 2 October 2021; Accepted 16 January 2022

ABSTRACT

Glyphosate is an organophosphorus herbicide, and has been widely used in agriculture. The glyphosate by-product salt is an intermediate product of glyphosate. The total phosphorus and total organic carbon contents of the by-product are high. Thus, achieved resource utilization is difficult. Attapulgite is often used as an adsorbent because of its large specific surface area and low price. In this study, a new strategy of phosphorus removal for glyphosate by-product salt utilization was developed by using attapulgite modified phosphorus removal agent. Three types of attapulgite, grey white–palygorskite clay (ATP1), opal–palygorskite clay (ATP2) and dolomitic–palygorskite clay (ATP3) were used for phosphorus removal by adsorption. The effects of attapulgite types, calcination temperature, chemical modification on the phosphorus removal from glyphosate by-product salt solution were studied. The modified attapulgite was characterized by scanning electron microscopy, energy-dispersive X-ray spectroscopy, X-ray diffraction and Fourier-transform infrared spectroscopy. The ATP3 was calcined at 700°C, and the total phosphorus removal rate can reach 96.96%. The phosphorus removal rate of Al and Fe loaded the third of attapulgite composite (Al/Fe-TATPIII) can reach 99.97%. The adsorption isotherm is consistent with the Langmuir model. The theoretical adsorption capacity reaches 14.59 mg g^{-1}, which conforms to the pseudo-second-order adsorption kinetic model.

Keywords: Glyphosate; By-product salt; Attapulgite; Modification

1. Introduction

Phosphorus is an essential nutrient for biological growth. A large amount of phosphorus-containing wastewater is generated during industrial and agricultural production, such as agricultural runoff, chemical production wastewater, and food processing wastewater. However, only about one tenth of the phosphorus discharged into the environment is consumed. Excess phosphorus can lead to eutrophication of water bodies, reduced dissolved oxygen concentration, and severe environmental pollution, which in turn leads to the death of aquatic animals [1]. There is also a large amount of phosphorus containing wastewater in the production process of glyphosate.

* Corresponding author.

Glyphosate is an organophosphorus herbicide composed of phosphoric acid and amino substances, and has been widely used in genetically modified crops [2]. It has characteristics of broad-spectrum and high-efficiency [3], and has the structural formula as shown in Fig.1.

Raw materials used to synthesize glyphosate are different. Thus, glyphosate synthesis methods are mainly classified into glycine method [4] and iminodiacetic acid (IDA) method [5]. In the process of synthesizing glyphosate by glycine method, a large amount of glyphosate mother liquor is produced. Commonly, NaOH is added into the mother liquor to recover triethylamine. However, this operation will cause the content of NaCl in the mother liquor of glyphosate to increase sharply, which makes the mother liquor difficult to deal with [6]. In addition, the glyphosate by-product salt can be obtained by evaporation and concentration of glyphosate mother liquor. However, it is difficult to use a resource due to the high total phosphorus (TP) and total organic carbon of glyphosate by-product salt, of which TP can reach 1,500–3,000 mg/kg. Therefore, the dephosphorization of glyphosate by-product salt is a key issue for its application in chlor-alkali industry. Nowadays, there are various methods for phosphorus removal, mainly classified into photocatalytic degradation [7], membrane separation [8], electrolysis [9], adsorption [10] and biological methods [11]. The adsorption method is widely used for phosphorus removal due to its simple operation, low requirements for equipment, low energy consumption, and high efficiency.

Activated carbon [12], biomass [13], metal oxides [14,15], and resins [16] are commonly used adsorbents. However, the above-mentioned adsorbents are expensive and lack of specificity for phosphate, which makes it difficult to be applied on a large scale [17]. The objective of this study is to prepare an adsorbent for removing phosphorus from glyphosate by-product salt wastewater. Attapulgite is a silicate mineral rich in magnesium and aluminum, with a silica tetrahedral structure [18,19]. Due to its large specific surface area, porous physical structure and excellent chemical structure, attapulgite can be used to prepare adsorbents [20–22]. Attapulgite resources are abundant in China, which is beneficial for the preparation of attapulgite adsorbent for phosphorus removal. However, natural attapulgite has great limitations in phosphorus removal, especially in the targeted removal of phosphorus impurities [23]. Therefore, a series of modification treatments are required to improve the adsorption performance of the attapulgite. Commonly, thermal modification [24–27], acid modification [28], salt modification [29] and organic modification [30] are used to modify the attapulgite to improve its adsorption capacity.

Attapulgite has a good cation exchange capacity. Thus, it can be loaded with metal ions [19]. Therefore, the attapulgite can be loaded with iron and aluminum salts, which have affinity for phosphorus to improve its phosphorus removal performance. At present, there have been related studies on phosphorus removal by modified attapulgite, mainly for the phosphorus removal from environmental wastewater and simulated wastewater [31]. However, there has been no report on the phosphorus removal from high-concentration by-product salt by glyphosate.

In this paper, the modification methods of attapulgite that can be used to remove phosphorus from glyphosate by-product salt and high-salt wastewater were discussed and compared, which provides a theoretical basis for the utilization of glyphosate by-product salt. In addition, effects of attapulgite type, calcination temperature and modification methods on the phosphorus removal from glyphosate by-product salt solution were studied, which provides a theoretical basis for the resource utilization of glyphosate by-product salt.

2. Experimental section

2.1. Reagents and materials

Three types of attapulgite, grey white palygorskite clay (ATP1), opal-palygorskite clay (ATP2) and dolomitic palygorskite clay (ATP3) were purchased from Changzhou Dingbang Mineral Products Technology Co., Ltd., (Jiangsu, China). Sodium hydroxide, potassium antimony tartrate, ammonium molybdate tetrahydrate, ascorbic acid, hexahydrate and aluminum chloride, ferrous sulfate heptahydrate supplied by Sinopharm Chemical Reagent Co., Ltd., (Shanghai, China) were of analytical grade. Sulfuric acid, ethanol and phenolphthalein were supplied by Nanjing Chemical Reagent Co., Ltd., (Nanjing, China). Glyphosate by product salt was supplied by HuBei XingFa Chemical Group Co., Ltd., China.

2.2. Material characterization

Crystal phase was recorded by X-ray diffractometer (XRD, X'Pert^3 Powder, Panalytical B.V., The Netherlands) with CuKα radiation (35 kV and 25 mA). Diffraction angles were measured for 2θ ranging from 5° to 85° at 0.1 s/step. Morphology and grain size were observed by scanning electron microscope (Nova NanoSEM 450, Thermo Fisher, America) operated at 15 kV. Elemental distribution was measured by energy-dispersive X-ray spectroscopy (Vantage DS1, Noran, America) attached to scanning electron microscope. The total phosphorus content in solution was determined using total phosphorus rapid tester (SH-50TN, Shengaohua, Jiangsu, China). X-ray diffraction (XRD) was used to determine the crystal phase composition of attapulgite, and scanning electron microscopy (SEM) was used to observe the microstructure of attapulgite. Composition of glyphosate by-product salt was estimated by the inductively coupled plasma atomic emission spectrometer (Perkin Elmer 4300DV, America). Table 1 shows the elemental composition of glyphosate by-product salt.

Table 1
Results of content determination of various elements in by-product salt of glyphosate

Elements	Content
P (mg/kg)	1,879.41
Ba (mg/kg)	0.034
Ca (mg/kg)	31.08
Fe (mg/kg)	2.82
Mg (mg/kg)	23.00
NaCl (g/kg)	931.00

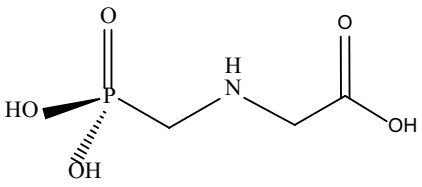

Fig. 1. Glyphosate structure.

As shown in Fig. 2, 3,471 cm^{-1} are telescopic vibration of –OH. 2,371 and 1,620 cm^{-1} are P–H and $–NH_2$ functional group vibration, respectively. 1,427 cm^{-1} is C–N functional group vibration. Therefore, it is presumed that the phosphorus in glyphosate by-product salt after calcination exists in the form of phosphite.

Fig. 3a shows the XRD patterns of three types of attapulgite. ATP1 is composed of quartz crystal phase and palygorskite crystal phase. ATP2 is composed of palygorskite calcite, montmorillonite, opal and quartz crystal phases. ATP3 is composed of dolomite, palygorskite and quartz crystal phase. The Fourier-transform infrared (FT-IR) spectra of ATP1, ATP2 and ATP3 are shown in Fig. 3b. The peaks at 898 and 918 cm^{-1} are attributed to Si–O–Si bonds in carbonate minerals. The peak at 3,749 cm^{-1} is O–H bond telescopic vibration.

2.3. Calcination of glyphosate by-product salt

The treated wastewater sample is prepared with a certain concentration of glyphosate by-product salt produced by Hubei Xingfa Chemical Group Company (Hubei, China).

2.4. Preparation of thermally modified attapulgite

Three types of attapulgite (ATP1, ATP2 and ATP3) were calcined at 400°C, 500°C, 600°C, 700°C, and 800°C for 2 h to obtain TATP1, TATP2 and TATP3, respectively.

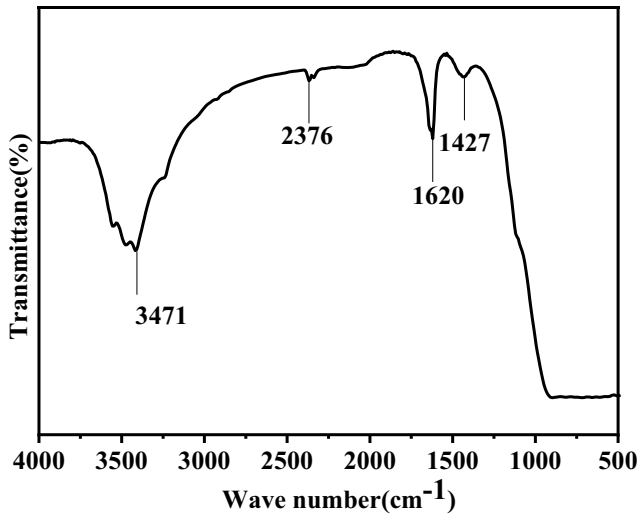

Fig. 2. FT-IR diagrams of glyphosate by-product salt.

2.5. Preparation of chemically modified attapulgite

5 g TATP3 calcined at 700°C was mixed with $FeSO_4·7H_2O$ according to the mass ratio of TATP3: Fe = 5:1. 100 mL water was added into, and was stirred in a magnetic stirrer at room temperature for 2 h. Then, it was filtered and washed, dried at 40°C, and ground to obtain Fe-TATP3. 5 g TATP3 calcined at 700°C was mixed with $AlCl_3·6H_2O$ according to the mass ratio of TATP3: Al = 5:1. 100 mL water was added into, and was stirred in a magnetic stirrer at room temperature for 2 h. Then, it was filtered and washed, dried at 40°C, and ground to obtain Al-TATP3. 5 g TATP3 calcined at 700°C was mixed with polymeric ferric sulfate according to the mass ratio of TATP3: PFS = 1:1. 100 mL water was added into, and was stirred in a magnetic stirrer at room temperature for 2 h. Then, it was filtered and washed, dried at 40°C, and ground to obtain PFS-TATP3. 5 g TATP3 calcined at 700°C

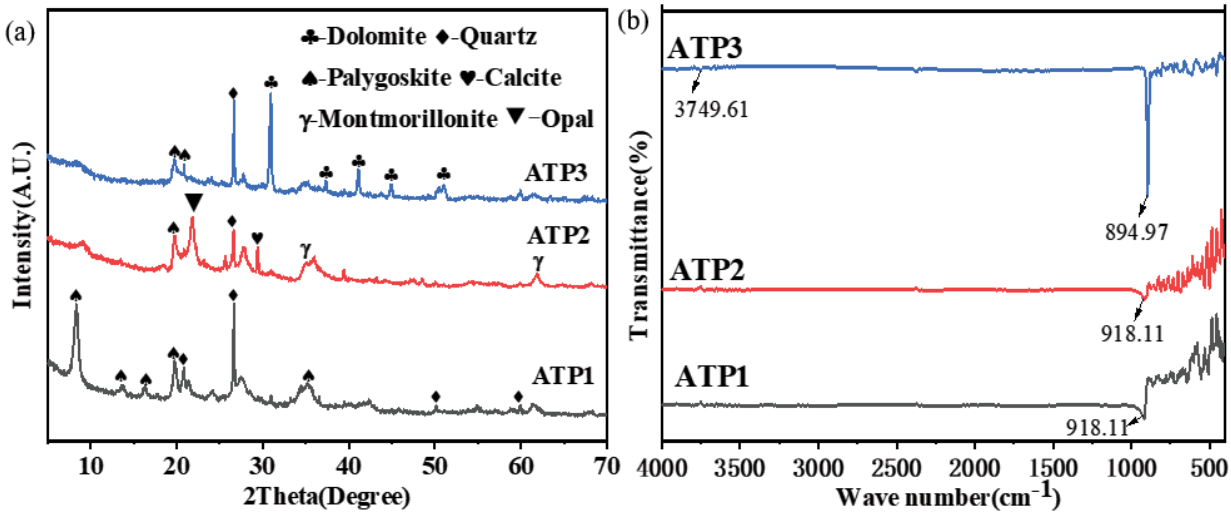

Fig. 3. (a) XRD patterns of three types of attapulgite and (b) FT-IR spectra of three types of attapulgite.

was mixed with $AlCl_3 \cdot 6H_2O$ and $FeSO_4 \cdot 7H_2O$ according to the mass ratio of TATP3: Al:Fe = 20:1:1, 10:1:1 and 5:1:1, respectively. 100 mL water was added into, and was stirred at room temperature in a magnetic stirrer for 2 h. Then, it was filtered and washed, dried at 40°C, and ground to obtain Al/Fe-TATPI, Al/Fe-TATPII and Al/Fe-TATPIII, respectively. Fig. 4 shows the preparation of the attapulgite adsorbent.

2.6. Adsorption experiments

The attapulgite was added into 10 g L^{-1} glyphosate by-product salt solution with magnetic stirrer according to 0.3 g/25 mL and then filtered for 2 h. The total phosphorus contents before and after the adsorption were measured, respectively. The total phosphorus removal rate and adsorption capacity were calculated according to the following equations.

The following equation is used to determine the phenol adsorbed per unit mass of adsorbent (q_{ads}).

$$q_{ads} = \frac{C_0 - C_e}{m_{adsorbant}} \times V_{sol} \quad (1)$$

where C_e and C_0 (mg L^{-1}) denote residual/final and initial concentrations of total phosphorus, respectively, V_{sol} is the volume of solution (L), and $m_{adsorbent}$ is the adsorbent mass (g).

The removal rate of total phosphorus Re (%) in solution is calculated by the following equation:

$$Re = \left[\frac{C_0 - C_e}{C_0}\right] \times 100 \quad (2)$$

2.7. Regeneration experiment

0.5 g of Al/Fe-TATPIII adsorbent was weighed separately and placed in 25 mL of 80 g L^{-1} glyphosate by-product salt solution for 3 h to obtain the equilibrium adsorption capacity q_e (mg g^{-1}). The reacted material was placed in 25 mL of ultrapure water, 0.1, 0.2 and 0.3 mol L^{-1} hydrochloric acid solution, shaken for 24 h. After washing the adsorbent, the above adsorption experiment was performed again to obtain the adsorption capacity q_d (mg g^{-1}). The regeneration rate was calculated according to Eq. (3).

$$Reg = \left[\frac{q_d}{q_e}\right] \times 100\% \quad (3)$$

2.8. Determination of ion exchange capacity

The cation exchange capacity (CEC) of attapulgite clay was determined by the ammonium chloride-anhydrous ethanol method [32]. The anion exchange capacity (AEC) was determined by titration method [33].

3. Results and discussion

3.1. Effect of calcination temperature on attapulgite

As shown in Fig. 5a, when the calcination temperature is below 600°C, the removal rate of total phosphorus by ATP1 decreases with the increase in calcination temperature. However, when the calcination temperature reaches 700°C, the removal rate of total phosphorus by ATP1 begins to increase with the increase in temperature. The removal rate of total phosphorus can reach 88.57%. When the calcination temperature reaches 800°C, the removal rate begins to decrease. The calcination is not conducive to total phosphorus removal rate of ATP2. The removal rates of total phosphorus of ATP2 with calcination are all lower than those without calcination, respectively. When the calcination temperature is below 700°C, the total phosphorus removal rate of ATP3 gradually increases with the increase of calcination temperature. When the calcination temperature is higher than 700°C, the total phosphorus removal rate begins to decrease. ATP3 achieves the best adsorption effect with the calcination temperature of 700°C, and the total phosphorus removal rate can reach 96.96%.

Fig. 5b shows the XRD patterns of ATP1 under different calcination temperatures. The palygorskite diffraction peak of ATP1 has no obvious change at the calcination temperature of 400°C. When the calcination temperature is further increased to 500°C, the palygorskite is significantly weakened, and when the calcination temperature reaches above 600°C, the palygorskite

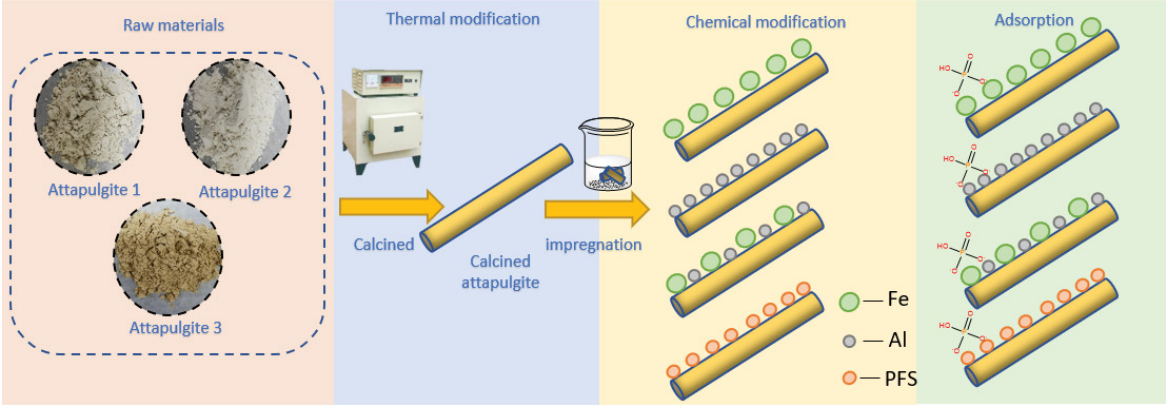

Fig. 4. Preparation and adsorption process of modified attapulgite.

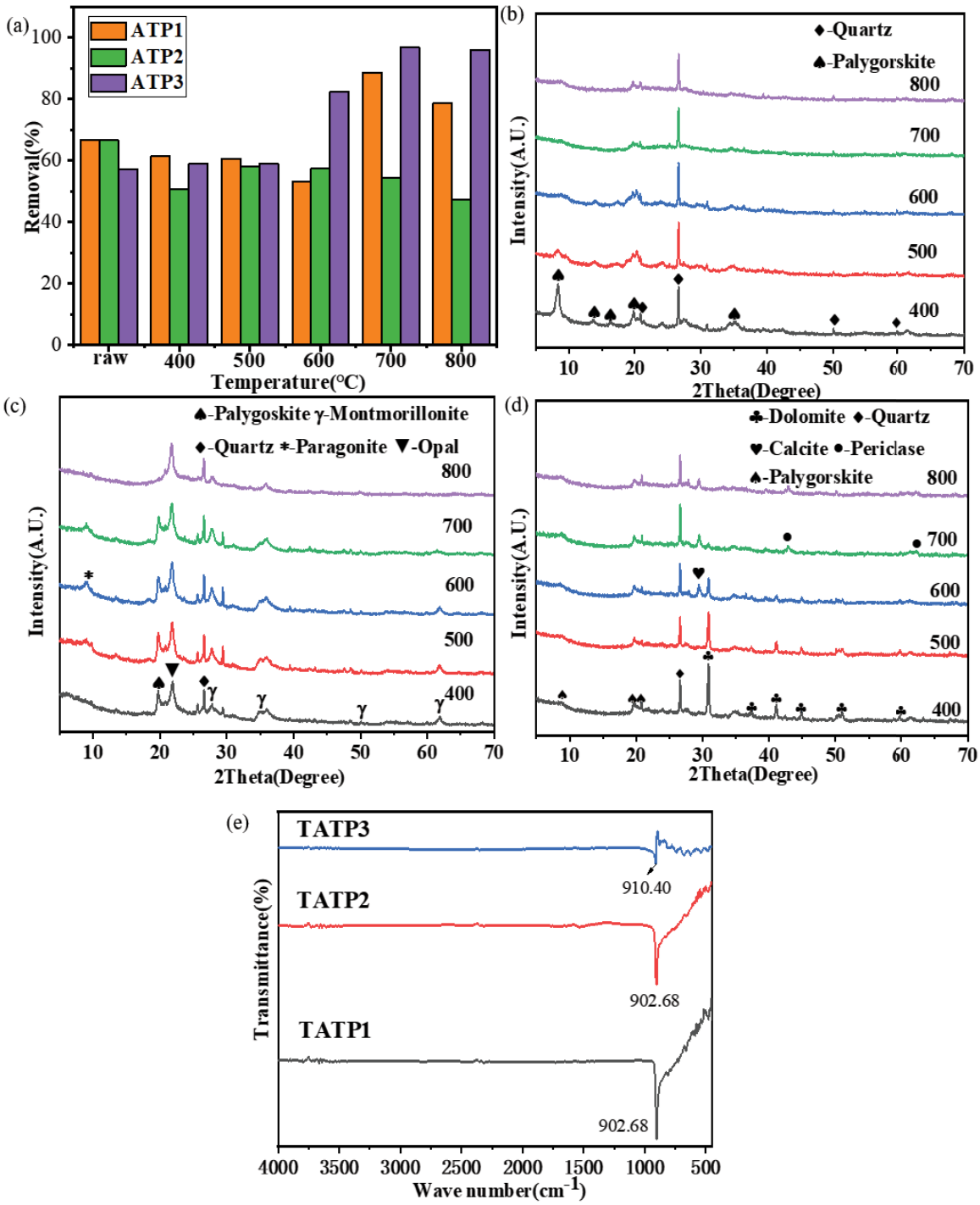

Fig. 5. (a) Effect of calcination temperature on phosphorus removal, (b) XRD pattern of ATP1 under different calcination temperatures, (c) effect of ATP3 calcination temperature on phosphorus removal, (d) XRD pattern of ATP3 under different calcination temperatures and (e) FT-IR of three types of attapulgite after calcination.

disappears completely. At calcination temperatures up to 800°C, the quartz diffraction peaks do not change significantly. With the increase of calcination temperature, the removal of crystalline water within the structure of the attapulgite causes the collapse of the pore structure of the palygorskite, resulting in the change of the palygorskite crystalline phase to amorphous, which leads to a decrease of the adsorption capacity.

Fig. 5c shows the XRD patterns of ATP2 under different calcination temperatures. The quartz and opal crystalline phases are stable and unchanging within the calcination temperature range of 800°C. At the calcination temperature

up to 800°C, the palygorskite diffraction peaks disappear completely. The paragonite diffraction peak appears at the calcination temperature of 600°C and disappears at the calcination temperature of 800°C. The montmorillonite diffraction peak begins to weaken with the increase of calcination temperature. When the calcination temperature reaches 800°C, the montmorillonite basically disappears and transforms into amorphous phase. Therefore, it is hypothesized that the decrease in the adsorption capacity of ATP2 with calcination temperature is due to the removal of crystalline water from attapulgite by high-temperature calcination, resulting in the collapse of the pore structure of palygorskite and the disappearance of the crystalline phase.

Fig. 5d shows the XRD patterns of ATP3 under different calcination temperatures. The crystalline phase composition of ATP3 does not change significantly at a calcination temperature of 500°C, and the total phosphorus removal rate increases significantly. When the calcination temperature is 600°C, the dolomite diffraction peak is transformed into the calcite, and the adsorption performance of ATP3 is significantly improved. When the calcination temperature is 700°C, the periclase diffraction peak appears. With the increase of calcination temperature, the calcite and periclase diffraction peaks gradually weakened. When the calcination temperature reaches 800°C, the calcite and periclase diffraction peaks completely disappear. The calcination of dolomite generated periclase and calcite are beneficial to the generation of calcium phosphate from phosphate, thus effectively improving the adsorption performance. Fig. 6 shows the process of decomposition of dolomite crystal structure occurring.

Fig. 5e shows the FT-IR of ATP1, ATP2 and ATP3 with calcination temperature of 700°C. A red shift of the Si–O–Si band of both ATP1 and ATP2 can be observed at 700°C, and the band at 902 cm^{-1} becomes sharp and intense. It may be because that Al atoms replace Si atoms, and the electronegativity of Al is smaller than that of Si, which reduces the vibration frequency and causes the red shift. In addition, the Si–O–Si bond peak of ATP3 shows a blue shift and becomes weaker at 910 cm^{-1}. This may be because that the calcination causes the Si–O–Si break, and the vibrational peak of Al–Mg–OH appears [27].

3.2. Effect of chemical modification on phosphorus removal

Fig. 6a shows the effect of different modifiers on the adsorption performance of the calcined ATP3. As shown in Fig. 6a, the phosphorus removal rate s of ATP3 by modification with four modifiers all reaches above 95%. Among them, the phosphorus remove rate of ATP3 with combined Fe/Al modification can reach 99.9%.

Fig. 6b shows the XRD patterns of TATP3 with calcination temperature of 700°C by modification with different modifiers. The crystalline phases of the Al and Al/Fe modifications does not change significantly. These two crystalline phases are present in water with calcium ions, and they form more calcium phosphate precipitates with phosphoric acid, thereby improving the adsorption performance of ATP3. The gismondine crystalline phase is formed in TATP3 modified with PFS, and the gypsum crystalline phase is formed in ATP3 modified with Fe. Fig. 6c shows the FT-IR patterns of TATP3 at calcination temperature of 700°C by modification with different modifiers. The IR spectrum is basically unchanged by modification with Al/Fe, PFS and Fe. Al-TATP3 shows a new peak at 540 cm^{-1}, which may be a stretching vibration of O–Si–O.

Fig. 6d shows the effect of Al/Fe ratio on the phosphorus removal rate. The best modification effect is achieved with the Al/Fe-TATPIII, and the removal rate can reach 99.97%. As can be seen from Fig. 7, the synthesis and adsorption process of Al/Fe-TATPIII is shown, the surface adsorbed water, bound water and zeolitic water are removed after calcination of attapulgite, which provides more adsorption sites for chemical modification.

Fig. 8a is a SEM image of ATP3. As shown in Fig. 8a, the surface of the ATP3 as needle-like structure is accumulated, which is due to the chain layer structure of the attapulgite. Fig. 8b is an SEM image of ATP3 with calcination temperature of 700°C. TATP3 still has the needle-like structure. However, the structure is shortened, and more disordered. Fig. 8c shows the SEM image of Al/Fe-TATPIII. The needle-like structure of the attapulgite disappears, and its surface is a rough irregular spherical structure stacked up. Fig. 8d is the energy-dispersive X-ray spectroscopy (EDS) image of Al/Fe-TATPIII. the iron element is successfully loaded onto the surface of the attapulgite.

3.3. Optimization of Al/Fe-TATP conditions on total phosphorus removal

3.3.1. Effect of waste salt concentration on phosphorus removal

Fig. 9a shows the effect of by-product salt concentration on adsorption capacity for phosphorus removal of three different mass ratios of Al/Fe. The adsorption capacity of all the three Al/Fe modifications increases gradually with the increase of glyphosate by-product salt concentration. When the by-product salt concentration is 10 g L^{-1}, the Al/Fe mass ratio has little effect on the adsorption capacity for phosphorus removal. With the further increase of the total phosphorus content, Al/Fe-TATPI gradually reaches the maximum adsorption capacity. The adsorption capacity may be related to the amount of Al/Fe addition. When the amount of Al/Fe addition increases, more Al and Fe are loaded on the surface of the attapulgite, and more ions can co-precipitate with phosphate, thereby a higher adsorption capacity can be obtained. The maximum adsorption capacities of the three adsorbents were 9.63, 10.05 and 13.67 mg g^{-1} respectively.

3.3.2. Effect of contact time on phosphorus removal

Fig. 9b shows the effect of contact time on the adsorption capacity for phosphorus removal. When the contact time is 120 min, the adsorption equilibrium is basically reached. When the contact time is 5 min, the amount of Al/Fe modifier addition has a greater effect on adsorption capacity. The greater the amount of Al/Fe addition, the higher the adsorption capacity. The adsorption capacities of Al/Fe-TATPI, Al/Fe-TATPII and Al/Fe-TATPIII reach 1.91, 1.24 and 2.03 mg g^{-1}, respectively. When the contact time is in the range of 10–30 min, the adsorption capacity of Al/Fe-TATPII

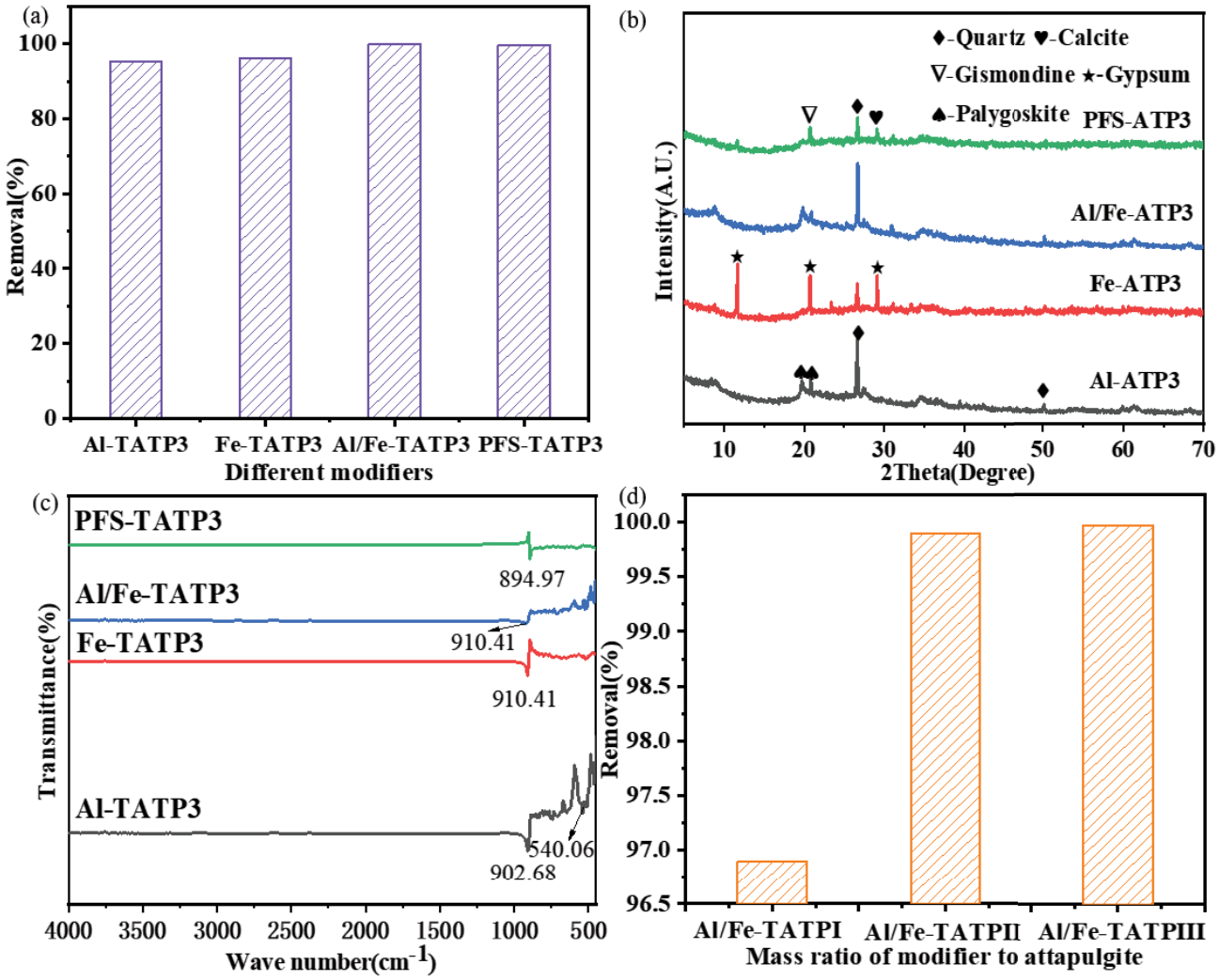

Fig. 6. (a) Effects of different modifiers on phosphorus removal rate, (b) XRD patterns of different modifiers, (c) FT-IR patterns of different modifiers and (d) effect of Al/Fe modifier ratio on phosphorus removal rate.

increases most rapidly. When the contact time is 240 min, the adsorption capacities of the three types of Al/Fe-TATP are relatively close, which are 2.28, 2.21 and 2.28 mg g^{-1}, respectively.

3.3.3. Effect of dosing amount on phosphorus removal

Fig. 9c shows the effect of Al/Fe-TATPIII dosing amount on the phosphorus removal of glyphosate by-product salt solution. When the adsorbent dose amount is in the range of 0.1–0.5 g/25 mL, the total phosphorus removal rate is greater than 99%. The adsorption capacity for phosphorus removal gradually decreases with the increase of dosage. This is because that the increase in dosage provides more adsorption sites, which leads to a decrease in adsorption capacity.

Fig. 10 shows the adsorption capacity of Al/Fe-TATPIII at different initial pH. The removal of total phosphorus was 98.43%–96% and adsorption capacity was 13.52–13.31 mg g^{-1} at the initial pH of the solution of 2–12, indicating that the prepared attapulgite adsorbent has good phosphorus removal in either acidic or alkaline solutions.

Table 2 shows the determination of the ion exchange capacity of ATP3 before and after modification. The results indicate that high temperature calcination and chemical modification can increase its anion exchange capacity.

3.4. Adsorption mechanism

3.4.1. Adsorption kinetics study

The investigate the interaction between phosphate molecules of the three modified adsorbents (Al/Fe-TATPI, Al/Fe-TATPII, Al/Fe-TATPIII) the pseudo-first-order and pseudo-second-order kinetic models were used, and the intraparticle diffusion model is used to analyze the control diffusion mechanism [34,35]. The three adsorption kinetic models are expressed as follows:

$$\ln(q_e - q_t) = \ln q_e - k_1 t \quad (4)$$

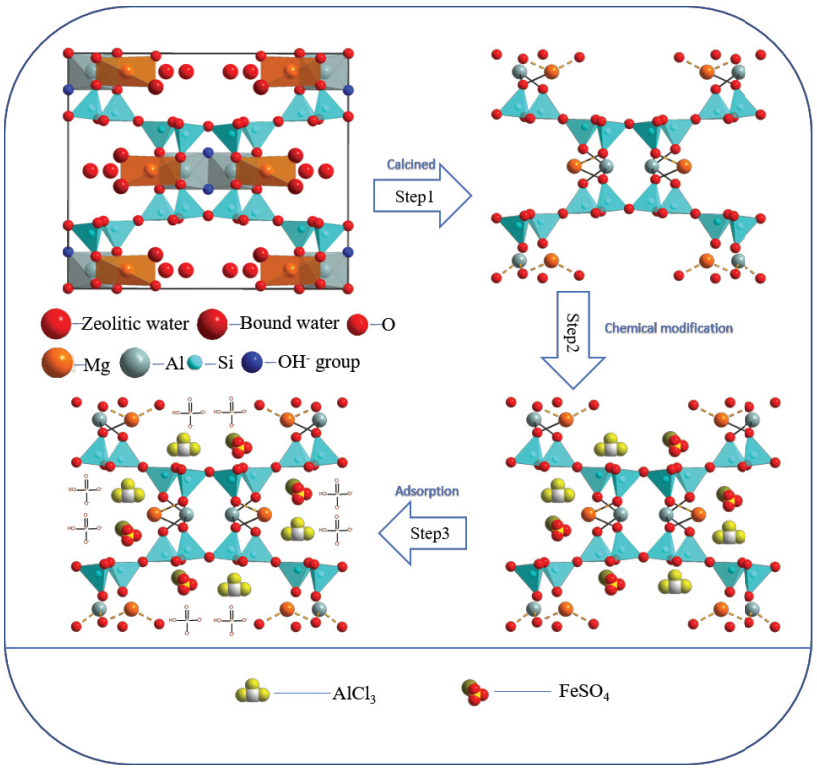

Fig. 7. Schematic illustration of preparation of Al/Fe-TATPIII and Al/Fe-TATPIII adsorption process.

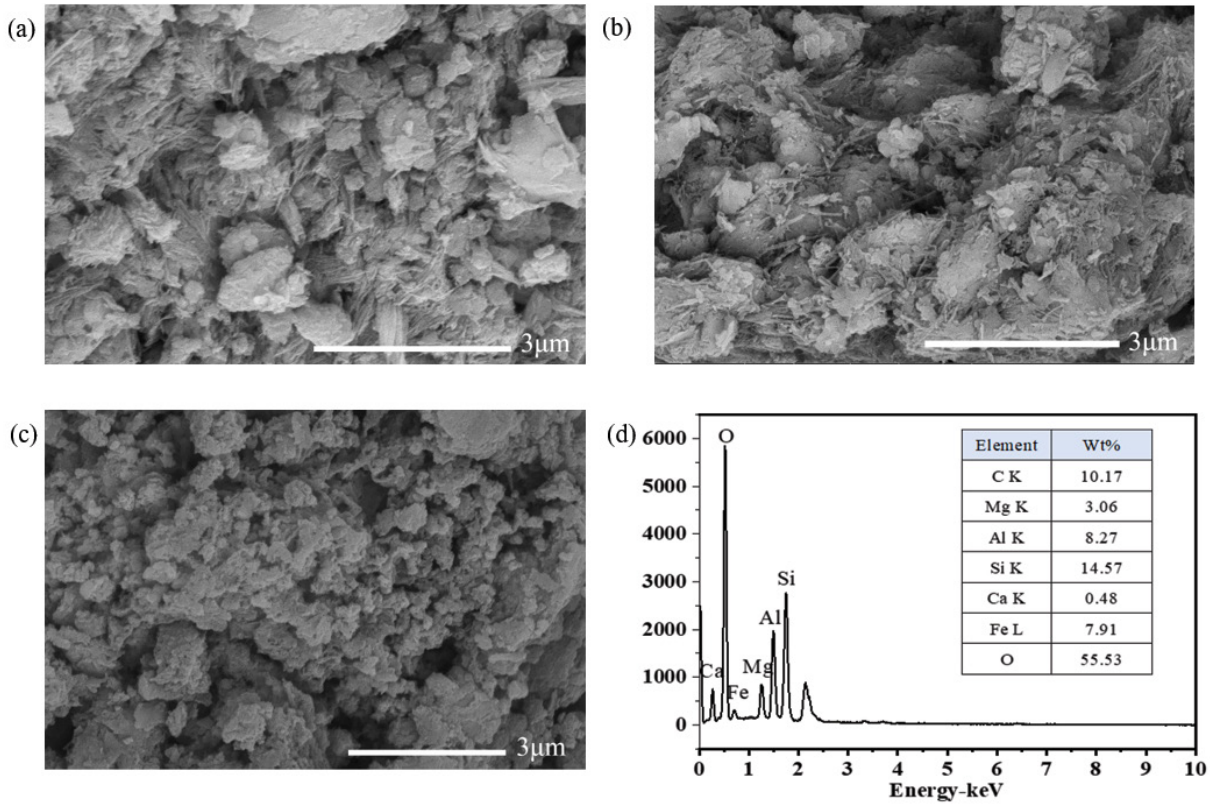

Fig. 8. Characterization result of ATP: (a) SEM of ATP3, (b) SEM of ATP3 with calcination temperature of 650°C, (c) SEM of Al/Fe-TATPIII and (d) EDS of Al/Fe-TATPIII.

$$\frac{t}{q_e} = \frac{1}{K_2 q_e^2} + \frac{1}{q_e} t \quad (5)$$

$$q_t = k_D t^{0.5} + C \quad (6)$$

The relevant parameters of the three models are shown in Table 3. The fitting curve as shown in the Fig. 11, the correlation coefficient R^2 of the pseudo-secondary dynamics model is closer to 1 than that of the pseudo-first-order kinetic model. In addition, the calculated value q_e of the pseudo-second-order model is closer to the experimental value than that of the pseudo-first-order kinetic model. This indicates that the pseudo-secondary dynamics model can better describe adsorption behavior, mainly chemical adsorption. Fig. 12 shows the kinetic data plotted according to the intra particle diffusion model. The observed adsorption kinetics consists of three continuous images. The first-stage 2.2 < $t^{0.5}$ < 5.5 $min^{0.5}$ represents the surface process, the second-stage 5.5 < $t^{0.5}$ < 11.0 $min^{0.5}$ represents the liquid-film diffusion, and the third stage observed 11.0 < $t^{0.5}$ < 15.5 $min^{0.5}$ represents that phosphate molecules diffuse through the gap to the active site of the adsorbent, so as to achieve adsorption equilibrium [36].

3.4.2. Adsorption isotherms

In this study, Langmuir model (7), Freundlich model (8) and Temkin model (9) three isothermal adsorption model equation was used to verify the interaction between of the three adsorbents (Al/Fe-TATPI, Al/Fe-TATPII, Al/Fe-TATPIII) and phosphate [15,22]. The fitting equation is as follows:

$$\frac{1}{q_e} = \frac{1}{K_L q_m C_e} + \frac{1}{q_m} \quad (7)$$

$$\log q_e = \ln K_F + \frac{1}{n} \log C_e \quad (8)$$

$$q_e = \left(\frac{RT}{b}\right) \ln A + \left(\frac{RT}{b}\right) \ln C_e \quad (9)$$

The fitting curves of Langmuir, Freundlich and Temkin models are shown in Figs. 13a, b and 14, respectively. The relevant parameters are shown in Table 4. The results show that the fitting parameters of Langmuir model are higher than those of other isothermal models, which indicates that phosphate exhibits monolayer adsorption on the heterogeneous phase points of adsorbents prepared with three different iron aluminum ratios [37]. According to Langmuir adsorption model, the maximum adsorption capacities of Al/Fe-TATPI, Al/Fe-TATPII, Al/Fe-TATPIII were 6.739, 8.646 and 14.59 mg g^{-1}, respectively. It was very close to the experimental values. Meanwhile, compared with Table 5, the maximum adsorption capacity of the adsorbent is the highest compared with the mineral adsorbent. Although the adsorption capacity of the adsorbent is lower than that of carbon nanotubes and resins, the preparation cost of the adsorbent using attapulgite as raw material is much lower than that of carbon nanotubes and resins.

3.5. Regeneration study

Fig. 15 shows the effect of different washing methods on the regeneration of the adsorbent. When regenerated with 0.1 mol L^{-1} HCl, the adsorbent regenerated best with a regeneration rate of up to 60.54% and pure water regeneration rate of up to 52.86%. It was tentatively proved that the adsorbent prepared with attapulgite has a certain recovery capacity.

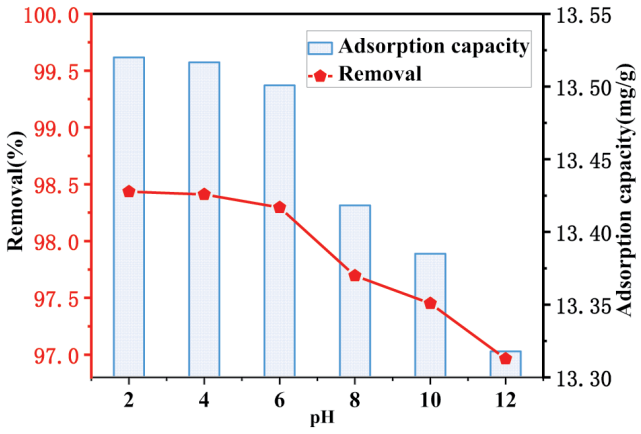

Fig. 10. Effect of initial pH of solution on the phosphorus removal rate.

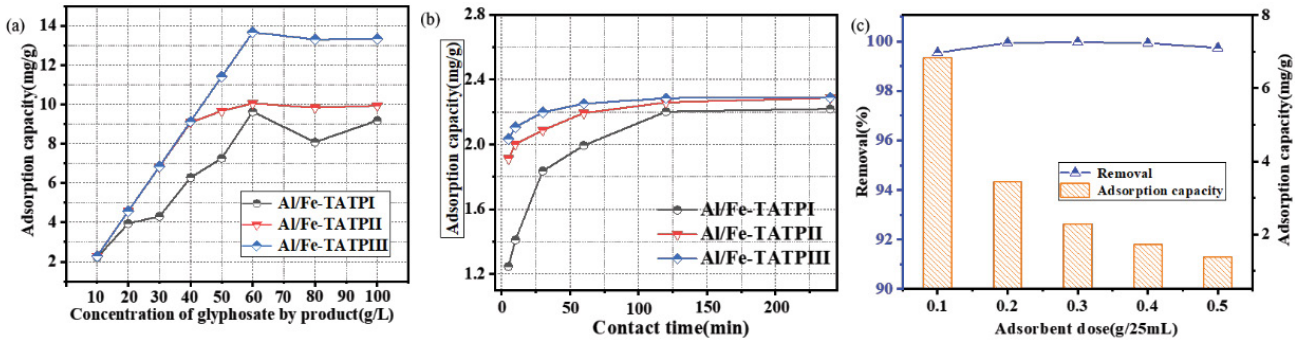

Fig. 9. (a) Effect of by-product salt concentration on the adsorption capacity for phosphorus removal, (b) effect of contact time on the adsorption capacity for phosphorus removal and (c) effect of adsorbent dose amount on the phosphorus removal rate.

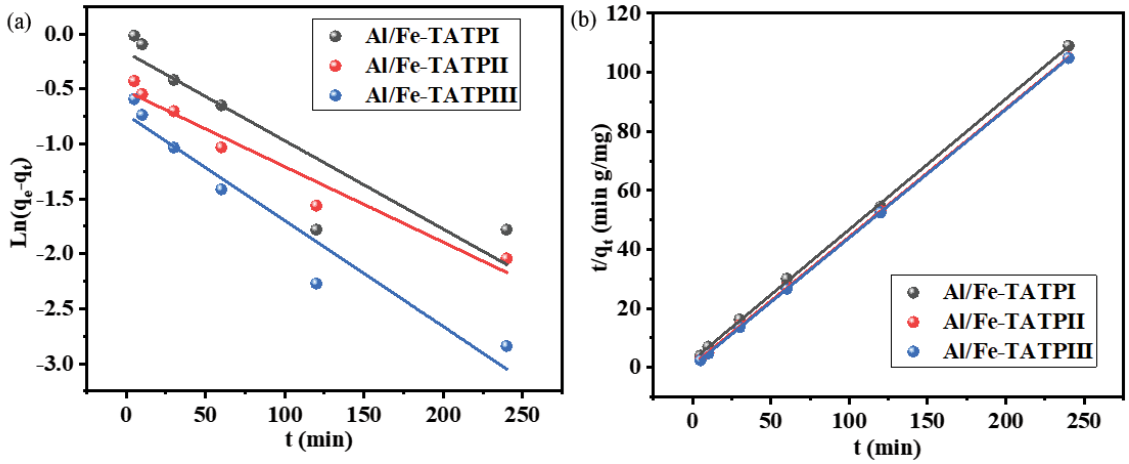

Fig. 11. Linear fitting of experimental data to (a) pseudo-first-order and (b) pseudo-second-order equations.

Table 2
CEC and AEC of attapulgite before and after modification

Adsorbent	CEC (mmol/100 g)	AEC (mmol g^{-1})
TATP3	11.67	5.00
700°C-TATP3	15.33	16.25
Al/Fe-TATPIII	4.33	20.00

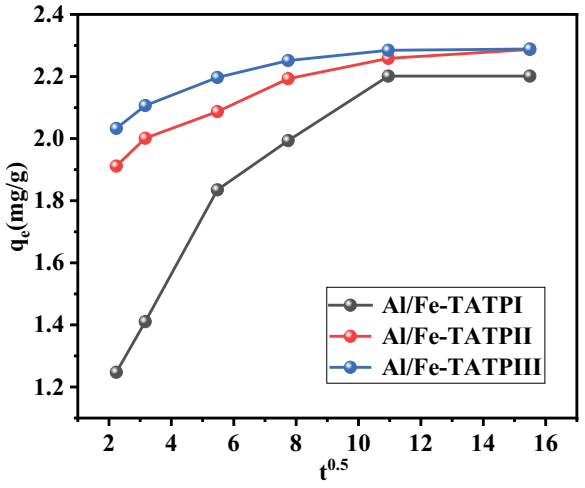

Fig. 12. Intraparticle diffusion of phosphate onto three adsorbents.

4. Conclusions

- Among the three types of attapulgite, only ATP3 can improve its phosphorus removal effect by high-temperature calcination. The optimal calcination temperature is 700°C, and the total phosphorus removal rate of glyphosate by-product salt solution can reach 96.96%.
- The effects of four types medium chemical modification on the phosphorus removal were studied. The total phosphorus removal rate of Al/Fe-TATPIII of glyphosate by-product salt solution can reach 99.97%.
- The chemical adsorption of Al/Fe-TATPIII determines the adsorption process for total phosphorus. When the contact time is 120 min, the adsorption balance can be achieved. Al/Fe-TATPIII adsorption process fits the Langmuir model, and the theoretical adsorption capacity can reach 14.59 mg g^{-1}. Regeneration rate of the adsorbent can reach 60%.

Funding

This work was supported by National Key Research and Development Program (Grant No. 2019YFC1905800) from China.

Acknowledgements

Thanks to Hubei Xingfa Chemical Group Co., Ltd. for providing glyphosate by-product salt.

Table 3
Fitting parameters of pseudo-first-order, pseudo-second-order kinetic model and intraparticle diffusion model

		Pseudo-first-order model			Pseudo-second-order model			Intraparticle diffusion model		
Adsorbents	$(q_e)_{exp}$ (mg g^{-1})	K_1 (min^{-1})	q_e (mg g^{-1})	R^2	K_2 (g mg^{-1} min^{-1})	q_e (mg g^{-1})	R^2	K_D	C	R^2
Al/Fe-TATPI	2.201	0.00805	0.848	0.819	0.0768	2.259	0.996	0.0725	1.270	0.8139
Al/Fe-TATPII	2.287	0.00688	0.596	0.955	0.2048	2.303	0.999	0.0277	1.914	0.8775
Al/Fe-TATPIII	2.289	0.00965	0.481	0.939	0.4422	2.292	0.999	0.01822	2.506	0.7767

Table 4
Fitting parameters of Langmuir, Freundlich and Temkin models

	Langmuir			Freundlich			Temkin		
Adsorbents	K_L (L mg^{-1})	q_m (mg g^{-1})	R^2	K_F (g mg^{-1} min^{-1})	$1/n$	R^2	A	b	R^2
Al/Fe-TATPI	5.599	6.739	0.949	3.209	0.173	0.906	4.215	1841.6	0.703
Al/Fe-TATPII	21.26	8.646	0.966	6.180	0.147	0.773	7280.9	3042.6	0.803
Al/Fe-TATPIII	19.809	14.59	0.970	9.905	0.174	0.615	5537.4	2086.8	0.540

Table 5
Comparison of the maximum uptake of various adsorbent for phosphate

Adsorbents	q_e (mg g^{-1})	Adsorbents	q_e (mg g^{-1})
4A zeolite	23 [38]	Modified bentonites	11.60 [39]
Multi-walled carbon nanotubes	198 [40]	Natural calcium-rich attapulgite	3.32 [41]
Ferrihydrite/bagasse composite	180.7 [42]	Monohydrocalcite	2.85 [17]
Lanthanum hydroxide-doped activated carbon fiber	15.3 [43]	Hydrated zirconia-loaded resin	47.21 [44]
Dendrite-like halloysite-zinc oxide nanocomposites	97.3 [45]	Zinc-based MOF/carbon nanotube hybrids	188.5 [46]
Zirconia functionalized SBA-15	13.77 [47]	$Al(OH)_3$ nanocrystals	850.5 [48]

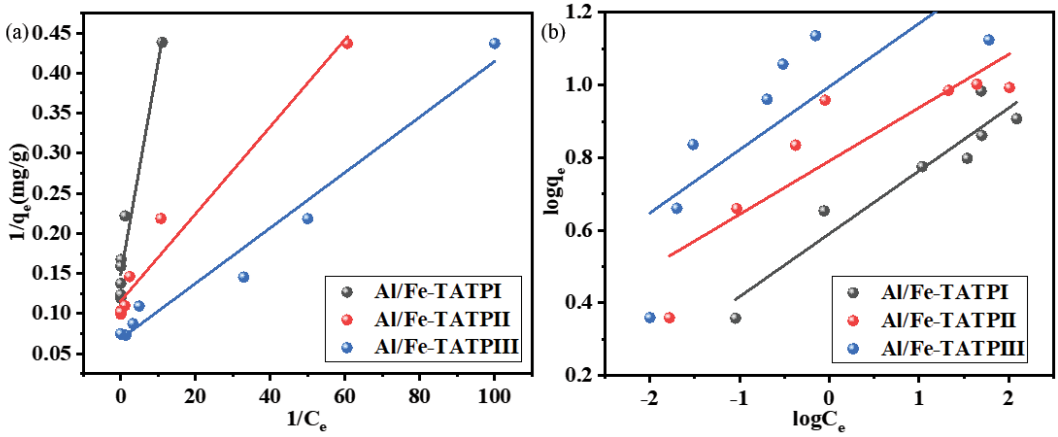

Fig. 13. Adsorption isotherm: (a) Langmuir adsorption and (b) Freundlich adsorption models.

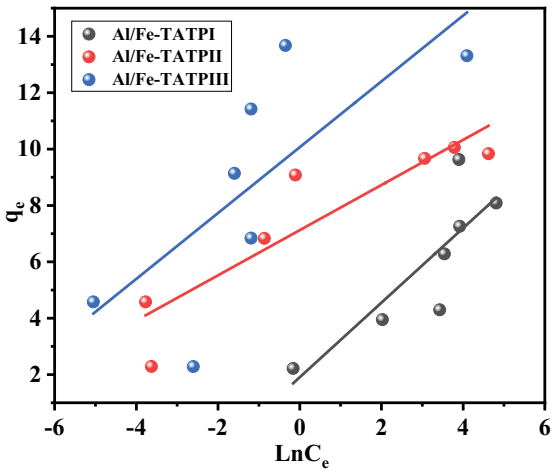

Fig. 14. Adsorption isotherm: Temkin model.

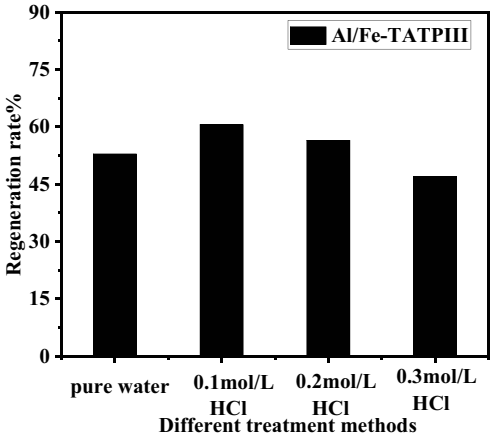

Fig. 15. Effect of different washing methods on regeneration performance of adsorbent.

References

[1] L.L. Cabral, I.C. Pereira, F. Perretto, A. Nagalli, R.C.P. Rizzo-Domingues, F.H. Passig, K.Q. de Carvalho, Adsorption and desorption of phosphate onto chemically and thermochemically pre-activated red ceramic waste: characteristics, batch studies, and mechanisms, J. Environ. Chem. Eng., 9 (2021) 106695, doi: 10.1016/j.jece.2021.106695.

[2] N. Lemke, A. Murawski, M.I.H. Schmied-Tobies, E. Rucic, H.-W. Hoppe, A. Conrad, M. Kolossa-Gehring, Glyphosate and aminomethylphosphonic acid (AMPA) in urine of children and adolescents in Germany – Human biomonitoring results of the German Environmental Survey 2014–2017 (GerES V), Environ. Int., 156 (2021) 106769, doi: 10.1016/j.envint.2021.106769.

[3] N. Botten, L.J. Wood, J.R. Werner, Glyphosate remains in forest plant tissues for a decade or more, For. Ecol. Manage., 493 (2021) 119259, doi: 10.1016/j.foreco.2021.119259.

[4] M. Xie, Z. Liu, Y. Xu, Removal of glyphosate in neutralization liquor from the glycine-dimethylphosphit process by nanofiltration, J. Hazard. Mater., 181 (2010) 975–980.

[5] J. Shen, J. Huang, H. Ruan, J. Wang, B. Van der Bruggen, Techno-economic analysis of resource recovery of glyphosate liquor by membrane technology, Desalination, 342 (2014) 118–125.

[6] Z. Liu, M. Zhu, P. Yu, Y. Xu, X. Zhao, Pretreatment of membrane separation of glyphosate mother liquor using a precipitation method, Desalination, 313 (2013) 140–144.

[7] H. Wu, Q. Sun, J. Chen, G.-Y. Wang, D. Wang, X.-F. Zeng, J.-X. Wang, Citric acid-assisted ultrasmall CeO_2 nanoparticles for efficient photocatalytic degradation of glyphosate, Chem. Eng. J., 425 (2021) 130640, doi: 10.1016/j.cej.2021.130640.

[8] X. Luo, J.-B. Zhang, L. He, X.-J. Yang, P.-Y. Lü, Analysis of the performance and mechanism of phosphorus removal in water by steel slag, Environ. Sci., 42 (2021) 2324–2333.

[9] X.-x. Wang, M. Wang, Y.-x. Jia, T.-t. Yao, The feasible study on the reclamation of the glyphosate neutralization liquor by bipolar membrane electrodialysis, Desalination, 300 (2012) 58–63.

[10] X. Li, L. Huang, H. Fang, M. Chen, Z. Cui, Z. Sun, D. Reible, Phosphorus adsorption by sediment considering mineral composition and environmental factors, Environ. Sci. Pollut. Res., 28 (2021) 17495–17505.

[11] Z. Fan, W. Zeng, Q. Meng, H. Liu, C. Ma, Y. Peng, Achieving partial nitrification, enhanced biological phosphorus removal and in-situ fermentation (PNPRF) in continuous-flow system and mechanism analysis at transcriptional level, Chem. Eng. J., 428 (2022) 131098, doi: 10.1016/j.cej.2021.131098.

[12] F.-F. Chen, H.-F. Li, X.-R. Jia, Z.-Y. Wang, X. Liang, Y.-Y. Qin, W.-Q. Chen, T.-Q. Ao, Characteristic and model of phosphate adsorption by activated carbon electrodes in capacitive deionization, Sep. Purif. Technol., 236 (2020) 116285, doi: 10.1016/j.seppur.2019.116285.

[13] X. Ma, B. Liu, M. Che, Q. Wu, R. Chen, C. Su, X. Xu, Z. Zeng, L. Li, Biomass-based hierarchical porous carbon with ultrahigh surface area for super-efficient adsorption and separation of acetone and methanol, Sep. Purif. Technol., 269 (2021) 118690, doi: 10.1016/j.seppur.2021.118690.

[14] T. Liu, K. Wu, L. Zeng, Removal of phosphorus by a composite metal oxide adsorbent derived from manganese ore tailings, J. Hazard. Mater., 217–218 (2012) 29–35.

[15] C. Li, Y. Li, Q. Li, J. Duan, J. Hou, Q. Hou, S. Ai, H. Li, Y. Yang, Regenerable magnetic aminated lignin/Fe_3O_4/$La(OH)_3$ adsorbents for the effective removal of phosphate and glyphosate, Sci. Total Environ., 788 (2021) 147812, doi: 10.1016/j.scitotenv.2021.147812.

[16] G. Xiao, Q. Meng, D151 resin preloaded with Fe^{3+} as a salt resistant adsorbent for glyphosate from water in the presence 16% NaCl, Ecotoxicol. Environ. Saf., 190 (2020) 110140, doi: 10.1016/j.ecoenv.2019.110140.

[17] S. Yagi, K. Fukushi, Removal of phosphate from solution by adsorption and precipitation of calcium phosphate onto monohydrocalcite, J. Colloid Interface Sci., 384 (2012) 128–136.

[18] M. Yang, J. Dai, L. Wang, Y. Li, Y. Song, First principles study of structural stability against the distribution of Mg and Al atoms and adsorption behaviors of heavy metals of attapulgite, Comput. Mater. Sci., 169 (2019) 109106, doi: 10.1016/j.commatsci.2019.109106.

[19] H. Wang, X. Wang, J. Ma, P. Xia, J. Zhao, Removal of cadmium(II) from aqueous solution: a comparative study of raw attapulgite clay and a reusable waste-struvite/attapulgite obtained from nutrient-rich wastewater, J. Hazard. Mater., 329 (2017) 66–76.

[20] L. Dong, H. Wang, Y. Huang, H. Chen, H. Cheng, L. Liu, L. Xu, J. Zha, M. Yu, S. Wang, Y. Duan, Elemental mercury removal from coal-fired flue gas using recyclable magnetic Mn-Fe based attapulgite sorbent, Chem. Eng. J., 407 (2021) 127182, doi: 10.1016/j.cej.2020.127182.

[21] W. Yan, D. Liu, D. Tan, P. Yuan, M. Chen, FT-IR spectroscopy study of the structure changes of palygorskite under heating, Spectrochim. Acta, Part A, 97 (2012) 1052–1057.

[22] P. Sun, W. Zhang, B. Zou, X. Wang, L. Zhou, Z. Ye, Q. Zhao, Efficient adsorption of Cu(II), Pb(II) and Ni(II) from waste water by PANI@APTS-magnetic attapulgite composites, Appl. Clay Sci., 209 (2021) 106151, doi: 10.1016/j.clay.2021.106151.

[23] R. Huang, Q. Lin, Q. Zhong, X. Zhang, X. Wen, H. Luo, Removal of Cd(II) and Pb(II) from aqueous solution by modified attapulgite clay, Arabian J. Chem., 13 (2020) 4994–5008.

[24] H. Yin, X. Yan, X. Gu, Evaluation of thermally-modified calcium-rich attapulgite as a low-cost substrate for rapid phosphorus removal in constructed wetlands, Water Res., 115 (2017) 329–338.

[25] H. Yin, M. Han, W. Tang, Phosphorus sorption and supply from eutrophic lake sediment amended with thermally-treated calcium-rich attapulgite and a safety evaluation, Chem. Eng. J., 285 (2016) 671–678.

[26] P.R. Christensen, J.L. Bandfield, V.E. Hamilton, D.A. Howard, M.D. Lane, J.L. Piatek, S.W. Ruff, W.L. Stefanov, A thermal emission spectral library of rock-forming minerals, J. Geophys. Res.: Atmos., 105 (2000) 9735–9739.

[27] A. Middea, T.L.A.P. Fernandes, R. Neumann, O. da F.M. Gomes, L.S. Spinelli, Evaluation of Fe(III) adsorption onto palygorskite surfaces, Appl. Surf. Sci., 282 (2013) 253–258.

[28] W. Zhang, L. Qian, Y. Chen, D. Ouyang, L. Han, X. Shang, J. Li, M. Gu, M. Chen, Nanoscale zero-valent iron supported by attapulgite produced at different acid modification: synthesis mechanism and the role of silicon on Cr(VI) removal, Chemosphere, 267 (2021) 129183, doi: 10.1016/j.chemosphere.2020.129183.

[29] H. Yin, P. Yang, M. Kong, W. Li, Use of lanthanum/aluminum co-modified granulated attapulgite clay as a novel phosphorus (P) sorbent to immobilize P and stabilize surface sediment in shallow eutrophic lakes, Chem. Eng. J., 385 (2020) 123395, doi: 10.1016/j.cej.2019.123395.

[30] C. Jia, Y. Mi, Z. Liu, W. Zhou, H. Gao, S. Zhang, R. Lu, Attapulgite modified with covalent organic frameworks as the sorbent in dispersive solid phase extraction for the determination of pyrethroids in environmental water samples, Microchem. J., 153 (2020) 104522, doi: 10.1016/j.microc.2019.104522.

[31] G.B. Douglas, D.P. Hamilton, M.S. Robb, G. Pan, B.M. Spears, M. Lurling, Guiding principles for the development and application of solid-phase phosphorus adsorbents for freshwater ecosystems, Aquat. Ecol., 50 (2016) 385–405.

[32] E.S. Kazak, A.V. Kazak, Experimental features of cation exchange capacity determination in organic-rich mudstones, J. Nat. Gas Sci. Eng., 83 (2020) 103456, doi: 10.1016/j.jngse.2020.103456.

[33] H. Ji, X. Song, C. He, C. Tang, L. Xiong, W. Zhao, C. Zhao, Root-soil structure inspired hydrogel microspheres with high dimensional stability and anion-exchange capacity, J. Colloid Interface Sci., 532 (2018) 680–688.

[34] D. Balarak, G. McKay, Utilization of MWCNTs/Al_2O_3 as adsorbent for ciprofloxacin removal: equilibrium, kinetics and thermodynamic studies, J. Environ. Sci. Health. Part A Toxic/Hazard. Subst. Environ. Eng., 56 (2021) 324–333.

[35] D. Balarak, M. Zafariyan, C.A. Igwegbe, K.K. Onyechi, J.O. Ighalo, Adsorption of Acid blue 92 dye from aqueous solutions by single-walled carbon nanotubes: isothermal, kinetic, and thermodynamic studies, Environ. Process., 8 (2021) 869–888.

[36] T.J. Al-Musawi, N. Mengelizadeh, O. Al Rawi, D. Balarak, Capacity and modeling of Acid blue 113 dye adsorption onto chitosan magnetized by Fe_2O_3 nanoparticles, J. Polym. Environ., 30 (2022) 344–359.
[37] S. Mor, K. Chhoden, P. Negi, K. Ravindra, Utilization of nano-alumina and activated charcoal for phosphate removal from wastewater, Environ. Nanotechnol. Monit. Manage., 7 (2017) 15–23.
[38] Q. Guan, L. Deng, D. Zhang, P. Ning, Z. Kong, L. He, Preparation of tetraethylenepentamine-functionalized 4A zeolite for effective removal of phosphate in water, Appl. Organomet. Chem., 34 (2020) 5861, doi: 10.1002/aoc.5861.
[39] M. Zamparas, A. Gianni, P. Stathi, Y. Deligiannakis, I. Zacharias, Removal of phosphate from natural waters using innovative modified bentonites, Appl. Clay Sci., 62–63 (2012) 101–106.
[40] S. Jiang, J. Wang, S. Qiao, J. Zhou, Phosphate recovery from aqueous solution through adsorption by magnesium modified multi-walled carbon nanotubes, Sci. Total Environ., 796 (2021) 148907, doi: 10.1016/j.scitotenv.2021.148907.
[41] H. Yin, M. Kong, Simultaneous removal of ammonium and phosphate from eutrophic waters using natural calcium-rich attapulgite-based versatile adsorbent, Desalination, 351 (2014) 128–137.
[42] R.-y. Zhou, J.-x. Yu, H.-x. Li, R.-a. Chi, Removal of phosphate from aqueous solution by ferrihydrite/bagasse composite prepared through in situ precipitation method, Colloids Surf., A, 603 (2020) 125144, doi: 10.1016/j.colsurfa.2020.125144.
[43] L. Zhang, Q. Zhou, J. Liu, N. Chang, L. Wan, J. Chen, Phosphate adsorption on lanthanum hydroxide-doped activated carbon fiber, Chem. Eng. J., 185–186 (2012) 160–167.
[44] H. Xu, W. Zeng, S. Li, B. Wang, Z. Jia, Y. Peng, Hydrated zirconia-loaded resin for adsorptive removal of phosphate from wastewater, Colloids Surf., A, 600 (2020) 124909, doi: 10.1016/j.colsurfa.2020.124909.
[45] Y. Wei, X. Liang, H. Wu, J. Cen, Y. Ji, Efficient phosphate removal by dendrite-like halloysite-zinc oxide nanocomposites prepared via noncovalent hybridization, Appl. Clay Sci., 213 (2021) 106232, doi: 10.1016/j.clay.2021.106232.
[46] Y. Wang, Z. Gao, Y. Shang, Z. Qi, W. Zhao, Y. Peng, Proportional modulation of zinc-based MOF/carbon nanotube hybrids for simultaneous removal of phosphate and emerging organic contaminants with high efficiency, Chem. Eng. J., 417 (2021) 128063, doi: 10.1016/j.cej.2020.128063.
[47] Y. Tang, E. Zong, H. Wan, Z. Xu, S. Zheng, D. Zhu, Zirconia functionalized SBA-15 as effective adsorbent for phosphate removal, Microporous Mesoporous Mater., 155 (2012) 192–200.
[48] Y. Song, X. Song, Q. Sun, S. Wang, T. Jiao, Q. Peng, Q. Zhang, Efficient and sustainable phosphate removal from water by small-sized $Al(OH)_3$ nanocrystals confined in discarded *Artemia* Cyst-shell: ultrahigh sorption capacity and rapid sequestration, Sci. Total Environ., 803 (2022) 150087, doi: 10.1016/j.scitotenv.2021.150087.